

Novel Phase Transformation in ZnO Nanowires under Tensile Loading

Ambarish J. Kulkarni,¹ Min Zhou,^{1,*} Kanoknan Sarasamak,² and Sukit Limpijumnong²

¹The George W. Woodruff School of Mechanical Engineering, Georgia Institute of Technology, Atlanta, Georgia 30332-0405, USA

²School of Physics, Suranaree University of Technology and National Synchrotron Research Center, Nakhon Ratchasima, Thailand

(Received 18 April 2006; revised manuscript received 18 June 2006; published 7 September 2006)

We predict a previously unknown phase transformation from wurtzite to a graphitelike ($P6_3/mmc$) hexagonal structure in $[01\bar{1}0]$ -oriented ZnO nanowires under uniaxial tensile loading. Molecular dynamics simulations and first principles calculations show that this structure corresponds to a distinct minimum on the enthalpy surfaces of ZnO for such loading conditions. This transformation is reversible with a low level of hysteretic dissipation of 0.16 J/m^3 and, along with elastic stretching, endows the nanowires with the ability to recover pseudoelastic strains up to 15%.

DOI: 10.1103/PhysRevLett.97.105502

PACS numbers: 61.50.Ks, 61.46.-w, 62.25.+g, 64.70.Nd

The assumption of crystal structures by a material reflects a complex interplay of intrinsic factors such as composition, band structure, valence electrons, bonding states, and structural symmetry and extrinsic factors such as temperature and loading. A change in any of these factors may trigger a transformation to a different structure, giving rise to polymorphism which is especially pronounced in compounds such as ZnO whose electronic bonding states show significant dependence on applied loading [1]. There are three hitherto well-known polymorphs of ZnO, including wurtzite (WZ, $P6_3mc$ space group), zinc blende (ZB, $F43m$) and rock salt (RS, $Fm\bar{3}m$) [2]. WZ is the most stable and commonly observed phase under ambient pressure. ZB can be obtained only on cubic surfaces under specific growth conditions. RS is the result of a transformation from WZ at pressures between 8–10 GPa [1,3–8]. This pressure-induced reversible transformation has received significant consideration primarily because hydrostatic compression is the most likely mode of loading for bulk ZnO. Recent work on GaN, MgO, and ZnO thin films has revealed a previously unknown unbuckled structure resulting from extensive surface reconstructions to suppress surface polarity [9–12]. So far, the existence of polymorphs other than WZ, ZB, and RS at various loading triaxialities has not been extensively studied.

Recent synthesis of quasi-1D nanostructures such as ZnO nanowires, nanobelts, and nanorods necessitates understanding of the response of ZnO to uniaxial tensile loading [13–15]. Since these nanostructures are single-crystalline and nearly defect-free, they are endowed with high strengths and the ability to undergo large deformations without failure. Also, their high surface-to-volume ratios enhance atomic mobility and promote phase transformations under loading along certain crystalline directions.

Here, we report a novel phase transformation from WZ to an unbuckled wurtzite phase (hexagonal, hereafter denoted as HX) within the $P6_3/mmc$ space group during uniaxial tensile loading of $[01\bar{1}0]$ -oriented ZnO nanowires [Fig. 1(a)]. This structure bears both resemblance to and distinction from the layered structure (LY) [9–12]; see

Fig. 1(c) which compares charge density distributions on the $(11\bar{2}0)$ planes of WZ, HX, and LY. The resemblance is in crystallography and the distinction is in coordination. Specifically, a strong bond along the $[0001]$ axis is seen in HX which occurs throughout the solid wires. In contrast, this interplanar bond is absent in LY, which extends only a few layers from the surface beneath which the structure is predominantly WZ. Therefore, despite the similar geomet-

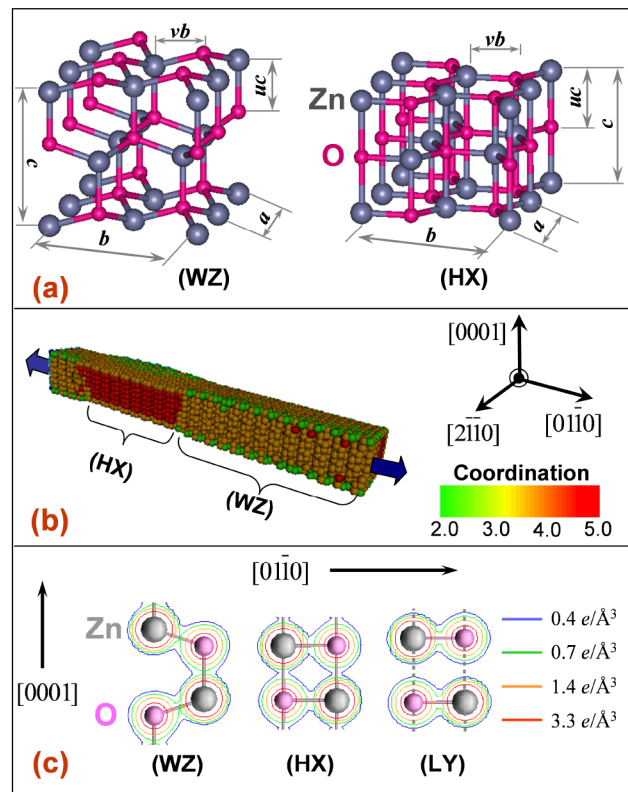


FIG. 1 (color online). (a) Wurtzite (WZ) and newly discovered hexagonal (HX) crystal structures, (b) nanowire with HX and WZ phases [transformation in progress under tensile loading (point C in Fig. 2 with a strain of 5.9%)]; and (c) charge density plots on the $(11\bar{2}0)$ planes of WZ, HX, and the layered structure (LY) reported in Refs. [9,10].

ric symmetries, HX has a higher coordination number (5) than LY (3). A similar HX phase has been reported as the natural state of boron nitride (*h*-BN) [16]. It has also been predicted as a metastable state of GaN during the WZ \rightarrow RS transformation at high pressures [17] and as a stable phase of MgO under hydrostatic tensile loading [18].

The deformation analysis here uses a quasistatic loading scheme within the molecular dynamics (MD) framework ([19]) and a Buckingham potential with charge interactions [20,21]. The parameters of the potential are the same as those in Ref. [22] and have been shown to accurately predict the lattice, elastic, and dielectric constants along with surface and defect properties of ZnO [20,22,23]. The nanowire considered has an initial WZ structure with [01 $\bar{1}$ 0] growth orientation and (21 $\bar{1}$ 0) and (0001) lateral surfaces. The lateral dimensions are 21.22×18.95 , 31.02×29.42 , or 40.81×39.89 Å. Under applied tensile stress (σ_b) along the wire axis, gradual transformation into the HX phase occurs. Figure 1(b) shows a partially transformed 21.22×18.95 Å wire containing both WZ and HX phases. To ascertain the relative energetic favorability of the two phases under loading, their enthalpies are independently determined using first principles calculations which are based on the density functional theory (DFT) as implemented in the VASP code [24], with local density approximation and ultrasoft pseudopotentials [25]. Computational parameters such as energy cutoff and sampling k points are the same as those in Ref. [7] which focused on the WZ \rightarrow RS transformation of ZnO and yielded lattice parameters, bulk modulus, and equilibrium transformation pressure that are in good agreement with experiments. For comparison, the emergence of HX as a stable phase under compressive loading (σ_c) along the [0001] axis is also shown.

We first characterize crystallographic changes associated with the transformation. As shown for the WZ lattice in Fig. 1(a), three parameters (a , c , and u) are typically used to define hexagonal structures, with uc denoting the offset between the Zn and O basal planes. Additional parameters b and v , with vb being the offset between Zn and O atoms along the [01 $\bar{1}$ 0] axis, are introduced to

delineate the difference between the HX and RS structures [7,17]. a , b , and c are the dimensions of the hexagonal unit cell along the [2 $\bar{1}$ 10], [01 $\bar{1}$ 0], and [0001] directions, respectively. Table I lists the lattice constants for WZ, HX, and RS structures. Note that the parameters for relaxed wires deviate slightly from the values for ideal bulk WZ due to surface effects [19,26]. For HX, $c = 4.35$ Å and $u = 0.50$ are similar to those for RS; whereas $a = 3.34$ Å and $v = 0.32$ are similar to those for WZ. Since v remains unchanged, HX has the same hexagonal symmetry around the c axis as WZ. During the transformation, u changes from its initial value of 0.38 for WZ to a value of 0.5 for HX (Table I), implying the flattening of the buckled wurtzite basal plane (Zn and O atoms becoming coplanar). As a result, Zn atoms are at equal distances from O atoms along the [0001] axis and the structure acquires the additional symmetry of a mirror plane perpendicular to the [0001] axis. This process occurs while the orientation of the basal plane remains invariant. The in-plane coordination of the HX structure is threefold and the full 3D coordination is fivefold (as compared to the fourfold in WZ). The formation of additional bonds (therefore the increase in coordination) along the [0001] axis can also be seen in the charge density distributions on (11 $\bar{2}$ 0) planes in Fig. 1(c). Obviously, an additional bond is formed between the Zn atom initially at the top left and the O atom initially at the bottom in the WZ structure. However, the charge density map for LY observed in [9,10] does not display such a strong intraplane molecular bond and the layers therein are only held together by Coulombic forces between Zn and O ions. Consequently, LY has a threefold in-plane coordination. The unusual fivefold coordination and uniform charge distribution around the atoms in HX and its crystallographic similarity to RS suggest that the WZ \rightarrow HX transformation observed here progresses toward an ionic bonding state with a higher coordination.

Figure 2 shows the tensile stress-strain (σ - ϵ) response of a nanowire with a 21.22×18.95 Å cross-section at 100 K. While only data for a particular wire size and temperature is shown here, the transformation and the characteristics of the σ - ϵ relation are the same for wires with lateral dimen-

TABLE I. Lattice parameters for WZ, HX, and RS under different loading conditions. Select values are highlighted in boldface for easy comparison across different structures.

Parameters	WZ						HX		RS
	DFT		EXP ^b	DFT		AP ^a	DFT	DFT	DFT
	$\sigma_b = 0$ GPa	$\sigma_b = 0$ GPa	$\sigma_b = 0$ GPa	$\sigma_b = 10$ GPa	$\sigma_c = -6$ GPa	$\sigma_b = 10$ GPa	$\sigma_b = 10$ GPa	$\sigma_c = -6$ GPa	$p = 8.22$ GPa
a (Å)	3.20	3.22	3.25	3.12	3.28	3.34	3.29	3.49	4.16
b (Å)	5.54	5.66	5.63	5.93	5.68	6.24	6.42	6.03	4.16
v	0.33	0.32	0.33	0.33	0.34	0.32	0.32	0.33	0.50
c (Å)	5.15	5.30	5.21	5.00	4.92	4.35	4.18	4.18	4.16
u	0.38	0.41	0.38	0.39	0.39	0.50	0.50	0.50	0.50
b/a	1.73	1.76	1.73	1.90	1.73	1.87	1.95	1.73	1.00
c/a	1.61	1.65	1.60	1.60	1.50	1.30	1.27	1.20	1.00

^aAnalytical Potential

^bExperiment [22]

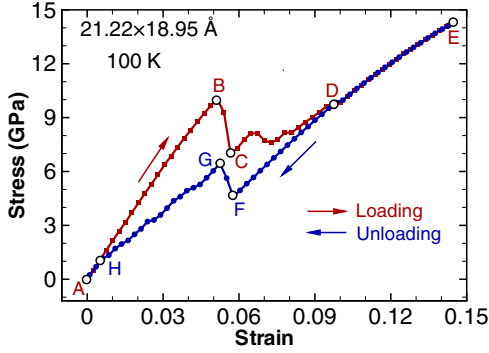


FIG. 2 (color online). Tensile stress-strain response of a $21.22 \times 18.95 \text{ \AA}$ nanowire at 100 K during loading-unloading. The hysteresis loop is relatively small.

sions between 18–40 Å and temperatures between 100–1200 K [27]. The region between A and B corresponds to elastic stretching of the WZ structure. Loading beyond B results in a stress drop from 10.02 to 6.98 GPa ($B \rightarrow C$) at $\epsilon = 5.14\%$. This softening behavior corresponds to the nucleation of the HX phase. At this stage, u shows a precipitous change to 0.5 and the Zn and O basal planes become coplanar. As the deformation progresses, the transformed region sweeps through the entire wire length ($C \rightarrow D$) and the transformation completes at $\epsilon = 9.71\%$ ($\sigma = 9.65$ GPa). Further deformation occurs through the elastic stretching of the transformed structure (HX) and ultimate fracture occurs at $\epsilon = 16\%$ ($\sigma = 15.29$ GPa, not shown) through cleavage along $\{\bar{1}2\bar{1}0\}$ planes. Unloading from any strain prior to the initiation of failure, e.g., point E with $\epsilon = 14.5\%$, is first associated with the recovery of the elastic deformation within the HX structure ($E \rightarrow F$). A reverse transformation from HX to WZ ($F \rightarrow G \rightarrow H$) initiates at $\epsilon = 5.77\%$ ($\sigma = 4.59$ GPa, point F) and completes at $\epsilon = 0.6\%$ ($\sigma = 1.15$ GPa, point H). Unloading beyond H occurs through elastic deformation within the WZ structure ($H \rightarrow A$). Strains up to 14.5% can be recovered, highlighting a very unusual aspect of the behavior of ZnO which normally is quite brittle. Obviously, the large recoverable strains observed here are associated with a unique structural transformation process which occurs only in $[01\bar{1}0]$ nanowires under uniaxial tensile loading. The energy dissipation associated with the stress-strain hysteresis loop is $\sim 0.16 \text{ J/m}^3$, much lower than that for the $\text{WZ} \rightarrow \text{RS}$ transformation in bulk ($\sim 1.38 \text{ J/m}^3$ with a maximum recoverable volumetric strain of 17% in compression) [3]. This low level of energy dissipation limits heat generation and heat-related damage, making the nanowires better suited for service under conditions of cyclic loading and large strains. It is important to point out that nanowires with other growth directions (e.g., $[0001]$) do not show such a phase transformation and are relatively brittle with failure strains not more than $\sim 7\%$.

To identify stable crystalline structures under uniaxial tensile loading along the $[01\bar{1}0]$ direction, we obtained their enthalpy as a function of c/a and b/a for specific

values of stress using DFT calculations. Since the transformation proceeds with the Zn and O basal planes becoming coplanar and a corresponding reduction in c , we also explored the stability of the HX phase under compression along the $[0001]$ axis. The enthalpy per unit cell (2 Zn-O pairs) under applied loading is given by

$$H(c/a, b/a) = E(c, b, a, u, v) - f_i q_i, \quad (1)$$

where E is the internal energy, $f_i q_i$ (summation not implied) is the external work, and f_i is the uniaxial force per unit cell. For tension along the b axis, $i = b$, $f_b = \sigma_b \times (ac)$, and $q_b = b$. For compression along the c axis, $i = c$, $f_c = \sigma_c \times (ab)$, and $q_c = c$. For each pair of c/a and b/a , u , v , and unit cell size a (thus the volume) are allowed to relax to minimize H . The minima of the $H(c/a, b/a)$ surface so obtained correspond to stable crystal structures under the applied stress.

Figure 3 shows the enthalpy surfaces (eV/unit cell) for $\sigma_b = 7, 10,$ and 13 GPa (with $\sigma_c = 0$ GPa) and $\sigma_c = -6$ GPa (with $\sigma_b = 0$ GPa). In each case, there are two minima. For the tensile loading, the first minimum (${}^b H_{\min}^{\text{WZ}}$) is in the vicinity of $c/a \approx 1.6$ and $b/a \approx 1.9$; for the compressive loading, the first minimum (${}^c H_{\min}^{\text{WZ}}$) is in the vicinity of $c/a \approx 1.5$ and $b/a = 1.732$; each corresponding to a WZ structure with lattice parameters slightly different from those at zero stress (Table I). The second minimum in each of these plots corresponds to the HX phase. For the tensile loading, the second minimum (${}^b H_{\min}^{\text{HX}}$) is in the vicinity of $c/a \approx 1.3$ and $b/a \approx 1.9$;

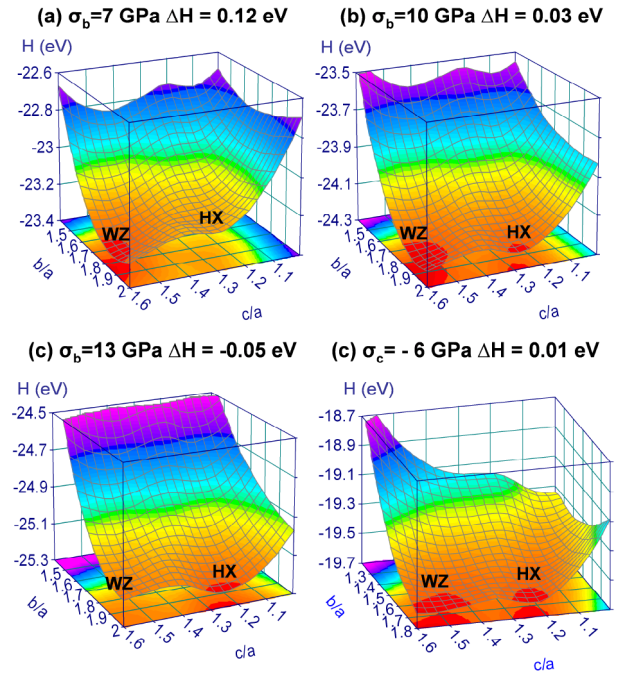


FIG. 3 (color online). Enthalpy surface maps from DFT calculations for uniaxial tensile stress of (a) $\sigma_b = 7$ GPa, (b) $\sigma_b = 10$ GPa and (c) $\sigma_b = 13$ GPa along the b axis and uniaxial compressive stress of (d) $\sigma_c = -6$ GPa along the c axis.

for the compressive loading, the second minimum (${}^c H_{\min}^{\text{HX}}$) is in the vicinity of $c/a \approx 1.2$ and $b/a = 1.732$. The structure at ${}^b H_{\min}^{\text{HX}}$ is that observed in the MD simulations discussed earlier. The difference in lattice parameters obtained from the two modes of loading stems from the fact that the ratio b/a is locked at 1.732 by structural symmetry under compression along the [0001] axis.

At a tensile stress of 7 GPa [Fig. 3(a)], ${}^b H_{\min}^{\text{WZ}}$ is much lower than ${}^b H_{\min}^{\text{HX}}$ ($\Delta H^b = {}^b H_{\min}^{\text{HX}} - {}^b H_{\min}^{\text{WZ}} = 0.12$ eV), hence, no transformation takes place. As the stress is increased to 10 GPa, ${}^b H_{\min}^{\text{HX}}$ and ${}^b H_{\min}^{\text{WZ}}$ become comparable ($\Delta H^b = 0.03$ eV) and consequently both WZ and HX are equally favored. At an applied stress of 13 GPa [Fig. 3(c)], ${}^b H_{\min}^{\text{HX}}$ is lower than ${}^b H_{\min}^{\text{WZ}}$ ($\Delta H^b = -0.05$ eV), indicating that HX is more stable. The transformation barrier between the two phases of 0.06 eV (0.05 eV if calculated using the analytic potential) is quite low, compared with the barrier of ~ 0.15 eV for the high pressure WZ \rightarrow RS transformation [7]. A similar behavior is observed under uniaxial compression along the [0001] direction. The WZ and HX enthalpy wells are comparable at $\sigma_c = -6$ GPa [$\Delta H^c = 0.01$ eV, Fig. 3(d)]. At higher compressive stresses, ${}^c H_{\min}^{\text{HX}}$ is lower than ${}^c H_{\min}^{\text{WZ}}$, indicating the relative favorability of HX under such conditions. As the magnitude of either σ_c or σ_b is increased above the corresponding equilibrium transition value, HX becomes more stable and the transformation barrier becomes even lower, resulting in an even higher driving force for transformation. In summary, the distinct minima in the vicinities of the HX and WZ structures on the enthalpy maps obtained through DFT calculations confirm what is discovered in MD calculations by pointing out that (1) HX is energetically favored over WZ above a critical applied tensile stress value of $\sigma_b \approx 10$ GPa along the [01 $\bar{1}$ 0] direction or a critical compressive stress value of $\sigma_c \approx -6$ GPa along the [0001] direction and (2) the barrier for the transformation decreases as applied stress increases.

HX can result from either uniaxial tension along the [01 $\bar{1}$ 0] direction or uniaxial compression along the [0001] direction because both cause interatomic distances in Zn and O basal planes to increase, creating conditions favorable for the two types of atoms to be accommodated in a single plane. This process is similar to the fcc \rightarrow bcc Bain transformation [17]. Phenomenologically, the transformation can be explained by considering the effect of structural distortion on the nature of bonding. Specifically, under the external stresses discussed, lattice parameters change and the interatomic Coulombic interactions favor ionic states of bonding over covalent states of bonding [2]. For example, hydrostatic pressure can cause the progression of WZ (moderately ionic) toward RS (highly ionic), as shown by both experiments and theoretical analyses [1,3–8].

Since HX and WZ can have very different properties, the stress-induced phase transformation may significantly alter the response of the nanowires. Examples include the

modulation of piezoelectric constant, Seebeck coefficient, and thermal conductivity [28]. Such effects provide mechanisms for tuning the response of nanocomponents in a variety of nano-electro-mechanical systems through the application of mechanical input.

Support from NSF (No. CMS9984298), NSFC (No. 10528205), NANOTEC (No. NN49-024) and TRF (No. BRG4880015 and No. PHD/0264/2545) is acknowledged. Computations are carried out at the NAVO and ASC MSRCs.

*To whom correspondence should be addressed.

Telephone: 404-894-3294.

Fax: 404-894-0186.

Email address: min.zhou@gatech.edu

- [1] C. H. Bates, W. B. White, and R. Roy, *Science* **137**, 993 (1962).
- [2] U. Ozgur *et al.*, *J. Appl. Phys.* **98**, 041301 (2005).
- [3] S. Desgreniers, *Phys. Rev. B* **58**, 14 102 (1998).
- [4] J. E. Jaffe and A. C. Hess, *Phys. Rev. B* **48**, 7903 (1993).
- [5] J. E. Jaffe *et al.*, *Phys. Rev. B* **62**, 1660 (2000).
- [6] H. Karzel *et al.*, *Phys. Rev. B* **53**, 11 425 (1996).
- [7] S. Limpijumnong and S. Jungthawan, *Phys. Rev. B* **70**, 054104 (2004).
- [8] J. Serrano *et al.*, *Phys. Rev. B* **69**, 094306 (2004).
- [9] F. Claeysens *et al.*, *J. Mater. Chem.* **15**, 139 (2005).
- [10] C. L. Freeman *et al.*, *Phys. Rev. Lett.* **96**, 066102 (2006).
- [11] J. Goniakowski, C. Noguera, and L. Giordano, *Phys. Rev. Lett.* **93**, 215702 (2004).
- [12] R. B. Capaz, H. Lim, and J. D. Joannopoulos, *Phys. Rev. B* **51**, 17 755 (1995).
- [13] C. Q. Chen *et al.*, *Phys. Rev. Lett.* **96**, 075505 (2006).
- [14] S. X. Mao, M. Zhao, and Z. L. Wang, *Appl. Phys. Lett.* **83**, 993 (2003).
- [15] Z. L. Wang, *J. Phys. Condens. Matter* **16**, R829 (2004).
- [16] R. M. Wentzcovitch *et al.*, *Phys. Rev. B* **38**, 6191 (1988).
- [17] S. Limpijumnong and W. R. L. Lambrecht, *Phys. Rev. Lett.* **86**, 91 (2001).
- [18] S. Limpijumnong and W. R. L. Lambrecht, *Phys. Rev. B* **63**, 104103 (2001).
- [19] A. J. Kulkarni, M. Zhou, and F. J. Ke, *Nanotechnology* **16**, 2749 (2005).
- [20] D. J. Binks and R. W. Grimes, *J. Am. Ceram. Soc.* **76**, 2370 (1993).
- [21] D. Wolf *et al.*, *J. Chem. Phys.* **110**, 8254 (1999).
- [22] D. J. Binks, Ph.D. thesis, University of Surrey, Harwell, 1994.
- [23] R. W. Grimes, D. J. Binks, and A. B. Lidiard, *Philos. Mag. A* **72**, 651 (1995).
- [24] G. Kresse and J. Furthmüller, *Comput. Mater. Sci.* **6**, 15 (1996).
- [25] D. Vanderbilt, *Phys. Rev. B* **41**, 7892 (1990).
- [26] A. J. Kulkarni and M. Zhou, *Acta Mechanica Sinica* **22**, 217 (2006).
- [27] A. J. Kulkarni *et al.* (unpublished).
- [28] A. J. Kulkarni and M. Zhou, *Appl. Phys. Lett.* **88**, 141921 (2006).